Biomedical Engineering

Mechanotransduction of Flow-Induced Shear Stress by Endothelial Glycocalyx Fibers is Torque Determined

Xiao Liu, Yubo Fan, and Xiaoyan Deng

To test the hypothesis that the mechanotransduction of flow-induced shear stress on endothelial cells (ECs) might be triggered by the total torque transmitted from the glycocalyx fibers to the ECs rather than by the total shear force acting directly on the membrane of ECs, we formulated the arterial wall as a five-layer model and numerically investigated the effect of two types of damages to the endothelial glycocalyx layer (EGL) on the flow in the EGL and on the drag force and bending moment acting on the glycocalyx fibers. One type of damage was to alter the thickness of the EGL, and the other was to damage its integrity. The results revealed that almost all amount of the shear stress acting on ECs was transmitted to the cells by the EGL and that the flow-induced shear stress acting directly on the cell membrane was negligibly small. In addition, the total force transmitted from the glycocalyx fibers to the cell membrane in the forms of drag force was hardly affected by the damages to the EGL. However, such damages could significantly influence the total torque at the roots of the EGL fibers. In conclusion, the mechanotransduction of shear stress by the EGL might be torque determined rather than force determined. *ASAIO Journal* 2011; 57:487–494.

Vascular endothelial cells (ECs) possess certain specific mechanotransducers that can respond to flow stimulus by converting physical stresses into biochemical signals.[1] Endothelial glycocalyx fibers have been proposed to be one of them to function in sensing flow.[2,3]

The endothelial glycocalyx is composed of proteoglycans, glycosaminoglycans such as heparan sulfate (HS), chondroitin/dermatan sulfate, hyaluronic acid, glycoproteins, and glycolipids that are firmly attached to the luminal surface of the ECs. Within the endothelial glycocalyx layer (EGL), endothelial glycocalyx harbors a wide array of blood-borne enzymes and proteins that are more dynamic and have a variety of functions.[4,5]

From the Key Laboratory for Biomechanics and Mechanobiology of the Ministry of Education, School of Biological Science and Medical Engineering, Beihang University, Beijing, China.

Supported by Grants-in-Aid from the National Natural Science Research Foundation of China (No. 11072023, 31170904) and the Innovation Foundation of BUAA for PhD Graduates.

Submitted for consideration November 2010; accepted for publication in revised form August 2011.

Reprint Requests: Xiaoyan Deng, PhD, School of Biological Science and Medical Engineering, Beihang University, Beijing 100191, China. Email: dengxy1953@buaa.edu.cn.

DOI: 10.1097/MAT.0b013e318233b5ed

Several theoretical studies investigated the effect of the EGL on the mechanotransduction in capillaries. Using simplified Brinkman equations with assumed parameters, Secomb *et al.*[6] demonstrated that flow-induced shear stress decayed rapidly with the distance from the outer edge of the EGL. Weinbaum *et al.*[3] verified the result based on the quasiperiodic ultrastructural model of the EGL proposed by Squire *et al.*[7] They also further investigated the drag force induced by the axial flow in the EGL and the deformation of the core proteins of the EGL using the classical beam theory. On the basis of a binary mixture theory, Wang[8] demonstrated that the degradation of the EGL could significantly reduce the drag force transmitted from the EGL to the ECs but enhance flow shear stress on the ECs. The aforementioned studies were mainly focused on small blood vessels (capillaries). In this study, we numerically stimulated the flow in relatively large arteries where atherosclerotic lesions in humans develop preferentially. Moreover, we proposed a new hypothesis to explain the experimental results by others[9–13] that only partial removing of the components of the EGL could significantly inhibit or even completely block the shear-induced nitric oxide (NO) production. The hypothesis believes that the mechanotransduction of shear stress on the endothelial surface by the EGL may be torque determined rather than force determined.

Methods

Geometry of the Model

The arterial segment concerned is simplified as a straight axisymmetric cylinder with a luminal radius (R_{lum}) of 3.1 mm and a longitudinal length (L) of 10 mm, as shown in **Figure 1A**.[14,15] The wall of the arterial segment is modeled as a five-layer structure. The thickness of each wall layer with the exception of the EGL is also shown in **Figure 1A**.[14,15] We assume that the EGL layer of the arterial wall is a structure of hexagonal symmetrical fibers,[3,5,16] as shown in **Figure 1**, **B** and **C**.

Numerical Approaches

Governing Equations. In this study, blood is considered as a homogeneous, incompressible Newtonian fluid, and all simulations are carried out under steady-state flow conditions.

Lumen. The flow simulation in the lumen of the arterial segment is based on the steady-state incompressible Navier-Stokes equations:

$$\rho(\boldsymbol{u} \cdot \nabla)\boldsymbol{u} + \nabla p - \mu\Delta\boldsymbol{u} = 0 \quad (1)$$

$$\nabla \cdot \boldsymbol{u} = 0 \quad (2)$$

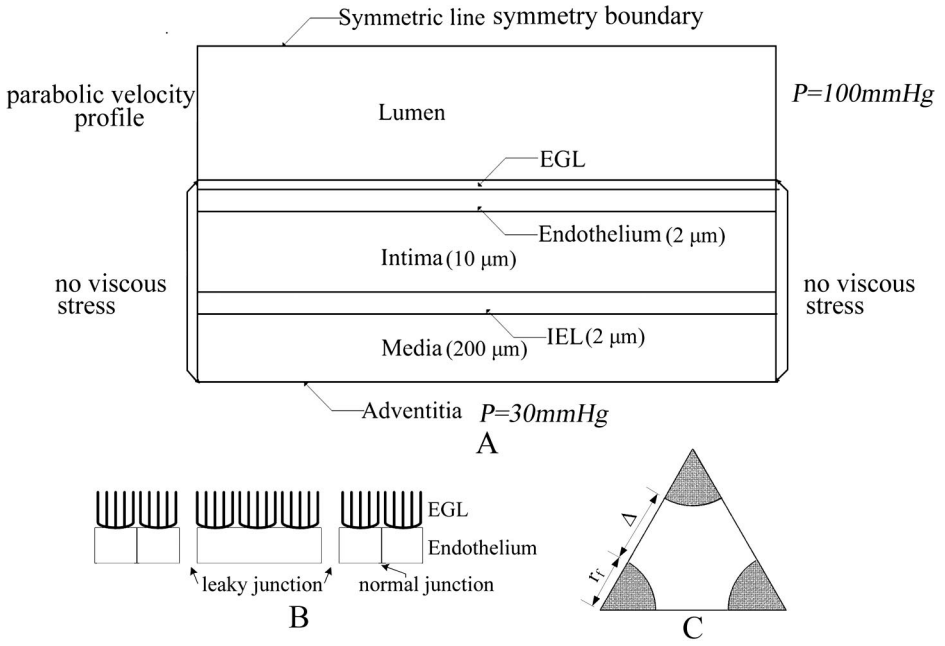

Figure 1. A: Schematic illustration of the computational geometry. Thickness of each layer of the artery except the endothelial glycocalyx layer (EGL) is illustrated in the parentheses. **B**: The EGL layer is structured with symmetrical fibers and leaky junctions. **C**: Sketch of the periodic unit of the idealized EGL fiber array observed *en face*.[16] The shaded areas are glycocalyx fibers, the radius of which (r_f) is taken as 6 nm and the open spacing (Δ) between which is 8 nm.

where **u** and p represent, respectively, the fluid velocity vector and the pressure. ρ and μ are the density and viscosity of blood ($\rho = 1050\ \mathrm{kg \cdot m^{-3}}$, $\mu = 3.5 \times 10^{-3}\ \mathrm{kg \cdot m^{-1} \cdot s^{-1}}$).

Arterial wall layers. The transmural flow across the arterial wall can be described by the Brinkman equation as follows[15,17]:

$$\frac{\mu_l}{K_l}\boldsymbol{u}_l = -\nabla P_l + \frac{\mu_l}{\varepsilon_l}\nabla^2 \boldsymbol{u}_l \tag{3}$$

$$\nabla \cdot \boldsymbol{u}_l = 0 \tag{4}$$

where $\mathbf{u}_l$ and p_l represent, respectively, the superficial velocity vector and the pressure based on the volume averaged method. ϵ_l and K_l are the porosity and the hydraulic permeability of the wall layer concerned. The subscript "l" denotes each layer of the arterial wall. For all layers, the viscosity of plasma μ_l is assumed to be 0.72×10^{-3} $\mathrm{kg \cdot m^{-1} \cdot s^{-1}}$.[14,15]

Parameters. To solve **Equation 3**, we have to acquire the values of the two parameters in the equations, namely the porosity (ϵ_l) and the hydraulic permeability (K_l) for each layer of the arterial wall. In this study, the porosity for the endothelium and the internal elastic lamina (IEL) is directly from experimental data by others,[18,19] and the others are obtained from their microstructures.

Parameters of the EGL. We assume that the EGL layer of the arterial wall is structured with symmetrical fibers and leaky junctions of cells that are either dying or in mitosis,[18,20] as shown in **Figure 1B**. As the leaky junctions only occupy a very small portion of the ELG layer, their effect on the porosity and the hydraulic permeability is ignored. The porosity of the EGL is then determined by the following equation[16]:

$$\varepsilon_{egl} = 1 - c = 1 - \frac{2\pi r_f^2}{\sqrt{3}(2r_f + \Delta)^2} \tag{5}$$

where c is the solid fraction of the EGL. r_f is the fiber radius (6 nm). Δ is the open spacing between fibers (8 nm). The calculated porosity for the EGL from **Equation 5** is 0.6735.

The hydraulic permeability of the EGL is obtained from the following equation[16]:

$$K_{egl} = \frac{R^2\left[\frac{\beta^2}{2} - \frac{\beta^4}{2} - \frac{3}{8} - \frac{1n(\beta)}{2}\right]\varepsilon_{egl}}{1-\beta^2} \tag{6}$$

where the outer radius of the fluid annulus [$R = 3^{1/4}(2r_f + \Delta)/\sqrt{2\pi}$, and [$\beta = r_f/R$. The calculated hydraulic permeability for the EGL from **Equation 6** is $6.0383 \times 10^{-18}\ \mathrm{m^2}$.

Parameters of the Endothelium. Filtration flow through the endothelium is assumed to move by both normal junctions and leaky junctions of the ECs. The hydraulic permeability (K_{end}) of the endothelium is then determined as follows:

$$K_{end} = K_{lj} + K_{nj} \tag{7}$$

$$K_{lj} = K_{slj}\frac{A_{lj}}{S} \tag{8}$$

where K_{slj} is the hydraulic permeability of one single leaky junction ($K_{slj} = w^2/3$), and A_{lj}/S is the fraction of the surface area S occupied by the leaky junctions. If a leaky cell is assumed to be located at the center of each periodic circular unit of radius ξ,[17] then A_{lj}/S is $(2\pi\ R_{cell})(2w)/(\pi\ \xi^2)$. As the

Table 1. Model Parameters for Each Layer

	EGL	Endothelium	Intima	IEL	Media
Hydraulic permeability, K (m^2)	6.0383×10^{-18}	1.7383×10^{-20}	4.2×10^{-17}*	4.3974×10^{-19}†	6.09×10^{-19}*
Porosity (ϵ)	0.6735	0.0005	0.8025*	0.002	0.258‡

* The parameters are from Dabagh *et al.*[17]
† The parameters are from Karner *et al.*[14] The rest are calculated.
‡ The parameters are from Yang and Vafai.[15]
EGL, endothelial glycocalyx layer.

fraction of the leaky junctions, ϕ, defined as the ratio of the area of leaky cells to the area of all cells ($\phi = R_{cell}^2/\xi^2$), can be determined from experimental results, **Equation 8** can be expressed as follows:

$$K_{lj} = \frac{4\ w^3}{3\,R_{cell}}\phi \tag{9}$$

For the normal junctions, the hydraulic permeability is as follows:

$$K_{nj} = L_{nj}\mu_l l_{end} \tag{10}$$

Where l_{end} is the thickness of the endothelium, $L_{nj} = 1.576 \times 10^{-9} m \cdot s^{-1} \cdot mm\ Hg^{-1}$ according to Tedgui and Lever.[21] From **Equation 7**, the hydraulic permeability of the endothelium can be calculated as $1.7383 \times 10^{-20}\ m^2$.

Parameters of the Intima. The intima is assumed to be a heterogeneous fiber matrix that is consisted of proteoglycan and collagen components.[17] According to the study by Dabagh *et al.*,[17] the porosity and hydraulic permeability of the intima can be taken as 0.8025 and $0.42 \times 10^{-16}\ m^2$, respectively.

The IEL and the Media. The IEL is assumed to have a constant thickness with fenestral pores. The media is modeled as a porous medium composed of smooth muscle cells. Their parameters are given in **Table 1**.

Boundary Conditions. As shown in **Figure 1A**, for the steady-state flow equations (**Equations 1–4**), the boundary conditions (BC) are as follows[14,15]:

BC-A:

At the inlet of the lumen of the arterial segment, the flow is set as a fully developed (parabolic) velocity profile ($u = U_0(1 - (r/R_{lum})^2)$), where U_0 is chosen as $676\ mm \cdot s^{-1}$, so that the resulting mean Reynolds number based on the radius of the artery is approximately 300.

BC-B:

The pressure at the outlet boundary of the artery lumen is set at 100 mm Hg. At the media-adventitia interface, a constant pressure boundary condition with 30 mm Hg is used.

BC-C:

Symmetric conditions are set at the axis of symmetry. No viscous flow is set on the remaining boundaries.

Computation Procedures. The numerical simulations are carried out using a validated finite element algorithm Comsol Multiphysics. Mesh independence is considered to be achieved when the difference in axial velocity of EGL between two successive simulations is <0.1%. For the cases in which the thickness of EGL is 0.1 μm, the computational mesh consists of 100 elements in radial direction and 400 elements in axial direction (100*400 quadratic elements) in lumen, 20*400 quadratic elements in the EGL, 20*400 quadratic elements in Endothelium, 16*400 quadratic elements in intima, 10*400 quadratic elements in IEL, and 30*400 quadratic elements in media layer. The same numbers of mesh elements are taken in all subdomains for other cases, except for EGL that contains 45*400, 80*400, and 150*400 quadratic elements when the thickness increases from 0.5 to 1.0 μm and 2 μm. The convergence criteria for all the fluid variables are 10^{-5}. The segregated solver was used in the simulations. For postprocessing, the axial velocity profile across the EGL at the middle of the segment is used to in all the cases.

Results

Flow within the EGL and the Resulting Drag Force and Torque on a Glycocalyx Fiber

Figure 2A gives the profiles of the axial velocity, $U(r)$ within the 0.1 μm EGL. As shown in the figure, the axial velocity decreases sharply along the glycocalyx fiber from the tip to the bottom (the solid line in **Figure 2A**). The axial velocity at the tip of the glycocalyx fibers (when $K_{egl} = 6.0383 \times 10^{-18}\ m^2$), $U(R)$, is approximately $4.27 \times 10^{-6}\ m \cdot s^{-1}$. However, the axial velocity at the location of 10 nm away from the tip is only 3.55% of $U(R)$. The value approaches a relatively constant value of only about $4.2 \times 10^{-12}\ m \cdot s^{-1}$ in the central region of the fiber. At the surface of ECs, the axial velocity decreases to $1.4 \times 10^{-14}\ m \cdot s^{-1}$. In addition, the calculation shows that the axial velocity scales linearly with the inlet velocity of the lumen (not shown in **Figure 2**).

The calculation shows that the flow-induced shear stress at the tip of the glycocalyx fiber is 1.53 Pa. However, as shown in **Figure 2A**, the shear stress (the gradient of the axial velocity with respect to r times the fluid viscosity) falls off dramatically along the glycocalyx fiber. As the axial velocity profile is relatively flat at the central region of the fiber, the lowest shear stress occurs there, which is about 1.4×10^{-9} Pa. The shear stress on the cell membrane is approximately 5.6×10^{-7} Pa. These results indicate that with the EGL, the value of flow-induced shear stress acting on the membranes of ECs is much smaller than that acting on the ECs without the EGL (1.53 Pa).

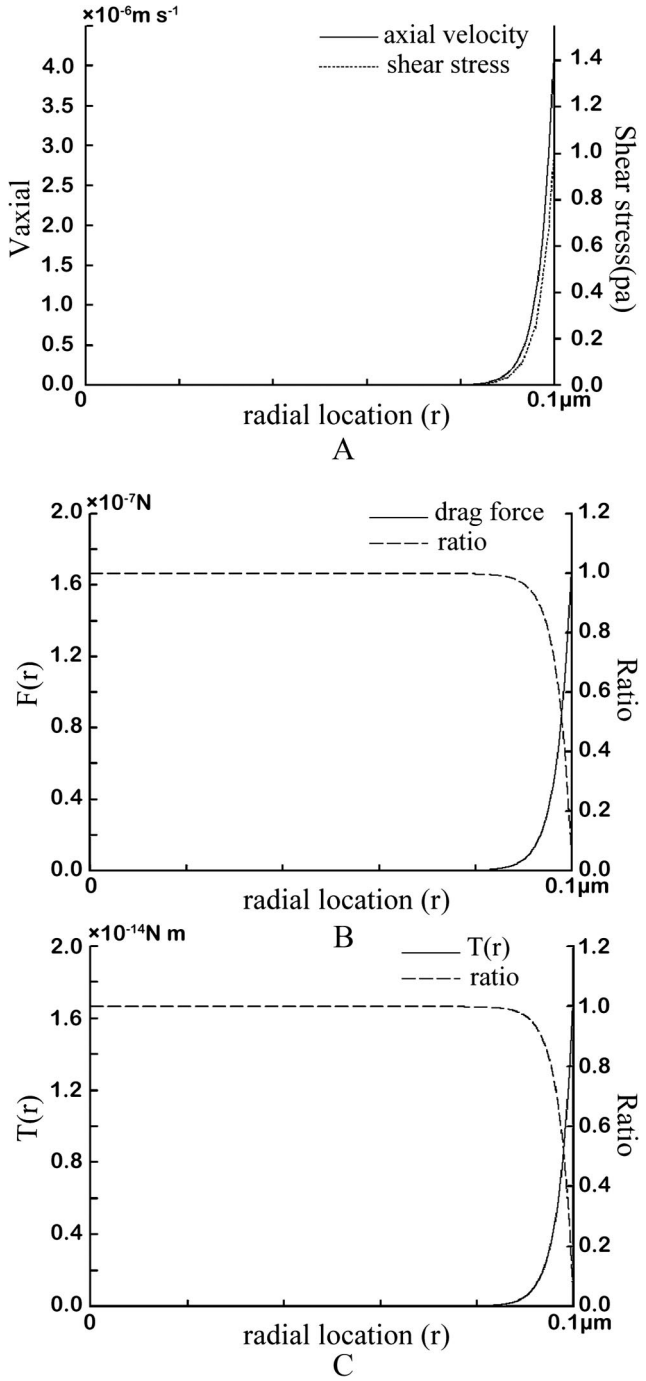

Figure 2. A: The axial velocity profile across the endothelial glycocalyx layer (EGL) in model with 0.1 μm EGL and K_{egl} = 6.0383 $\times$ 10^{-18} m^2. The dotted line shows the profile of shear stress along the EGL. **B**: The profile of the local drag force per unit fiber length ($F(r)$) along the EGL fiber. The dashed line demonstrates the ratio of the integrated $F(r)$ from the tip of the fiber R to the location r to the total $F(r)$ on the fiber. **C**: The solid line illustrates the profile of the bending moment per unit length $T(r)$ acting on the root of the glycocalyx fiber. The dashed line shows the integrated $T(r)$ from the tip of the fiber R to the location r to the total $T(r)$ on root of the fiber.

The axial flow in the EGL can result in a drag force on the glycocalyx fiber. The local drag force per unit fiber length, $F(r)$, acting on each glycocalyx fiber can be estimated using the quasiperiodic ultrastructural model (**Figure 1C**) of the EGL

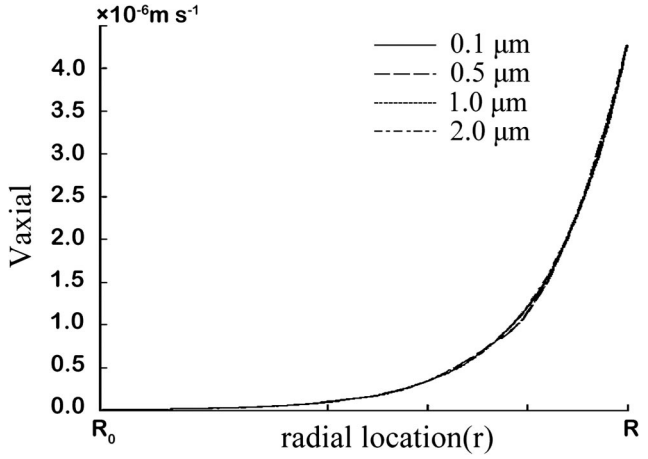

Figure 3. Profile of the axial velocity from the tip of the fiber R to $R_0 = R - 20$ nm with different endothelial glycocalyx layer (EGL) thickness in models with K_{egl} = 6.0383 $\times$ 10^{-18} m^2.

proposed by Squire *et al.*[7] and used by Weinbaum *et al.*[3] in the calculation of $F(r)$:

$$F(r) = \frac{\pi \mu_1 U(r)\ r_f^2}{c \quad K_{egl}} \tag{11}$$

where c is the solid fraction of the EGL calculated by **Equation 5**, r_f is the fiber radius (6 nm), and $U(r)$ is the axial velocity as a function of radial location in the EGL as shown in **Figure 2A**.

Figure 2B shows the profile of the drag force per unit fiber length $F(r)$ acting on a glycocalyx fiber. $F(r)$ decreases rapidly along the glycocalyx fiber from the tip to the root. When K_{egl} = 6.0383 $\times$ 10^{-18} m^2, approximately 96.4% of the total drag force acts on the 10-nm tip section of a 0.1 μm glycocalyx fiber (the dotted line in **Figure 2B**). The total drag is 5.33 $\times$ 10^{-4} pN.

The bending moment per unit length $T(r)$ acting on the root of the glycocalyx fiber can be obtained as $T(r) = F(r) \cdot r$. As illustrated in **Figure 2C**, similar to $F(r)$, $T(r)$ also drops sharply along the glycocalyx fiber from the tip. The dashed line in **Figure 2C** demonstrates that almost all the bending moment on the root of the glycocalyx fiber is obtained from the tip section. The total torque of a fiber with 0.1 μm is 5.17 $\times$ 10^{-2} pN $\cdot$ nm.

Effect of EGL Thickness

Up to now, numerous studies have been carried out to determine the thickness of the EGL for different blood vessels. It has been documented that for microvessels, the thickness of the EGL ranges from <0.1[5] to 0.5 μm.[22] As for larger blood vessels, it is between 0.7 and 4 μm,[23–25] depending on species and the size of the blood vessel. The EGL is made up of a firm layer and a dynamic layer with a much looser structure.[5] In this study, we only consider the firm layer of the EGL in our model assuming that the dynamic layer has little effect on the flow due to its loose structure. On the basis of the aforementioned EGL measurement data, we assume an EGL thickness from 0.1 to 2 μm in our model.

Figure 3 shows the axial velocity profile within 20 nm of the edge of EGL with different EGL thickness. As evident from the

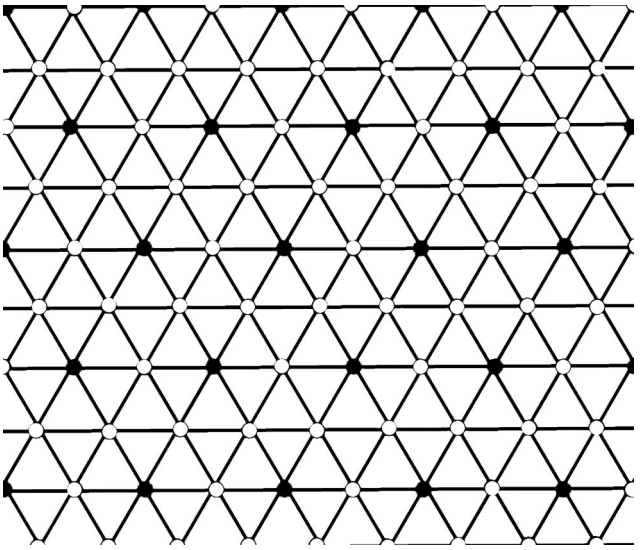

Figure 4. Schematic illustration of damages in endothelial glycocalyx layer (EGL) integrity. The black and the white circles are the glycocalyx fibers of the intact model. The white circles are removed in the damaged model, and the black circles are the glycocalyx fibers of the damaged model. The open spacing between fibers varies from 8 to 28 nm.

figure, the axial velocity of the tip section of the glycocalyx fiber is almost the same for the models with different EGL thickness.

The total drag force acting on a glycocalyx fiber depends slightly on the effect of the EGL thickness. When the EGL thickness increases from 0.1 to 0.5 μm and 1.0 μm, the total drag force increases slightly from 5.33×10^{-4} to 5.49×10^{-4} pN and 5.74×10^{-4} pN. However, the total drag force on the 2.0 μm glycocalyx fiber decreases to 4.12×10^{-4} pN. In contrast, the EGL thickness can significantly affect the total torque on the root of a glycocalyx fiber. For instance, the total torque is 0.273, 0.572, and 0.822 pN · nm, respectively, when the thickness increases from 0.5 to 1.0 μm and 2.0 μm.

Effect of EGL Integrity

To simulate damages of EGL integrity, we assume that the hexagonal symmetrical structure of the model remains intact, but the middle fiber of every three fibers along rays leaving each undamaged fiber toward its closest neighbors is removed. Therefore, as shown in **Figure 4**, the open spacing between fibers enlarges from 8 to 28 nm ($2\Delta + 2r_f$), and the total of fibers is only one quarter of the intact model. The porosity and hydraulic permeability of the damaged EGL are recalculated from **Equations 5** and **6**, which is 0.9184 and 1.2852×10^{-12} m^2, respectively.

The calculated results show that damages to the EGL can significantly enhance the total drag force on the glycocalyx fiber and the total torque on the root of the fiber. The total drag on a 0.1 μm fiber increases four times to 2.12×10^{-3}pN from the value of 5.33×10^{-4} pN and the total torque on the root of a fiber increases to 0.187 pN · nm. Moreover, as shown in **Figure 5**, the damage to the EGL alters the distribution of the drag force along a fiber and the corresponding bending moment. As a result, if the EGL is damaged, the ratio of the drag

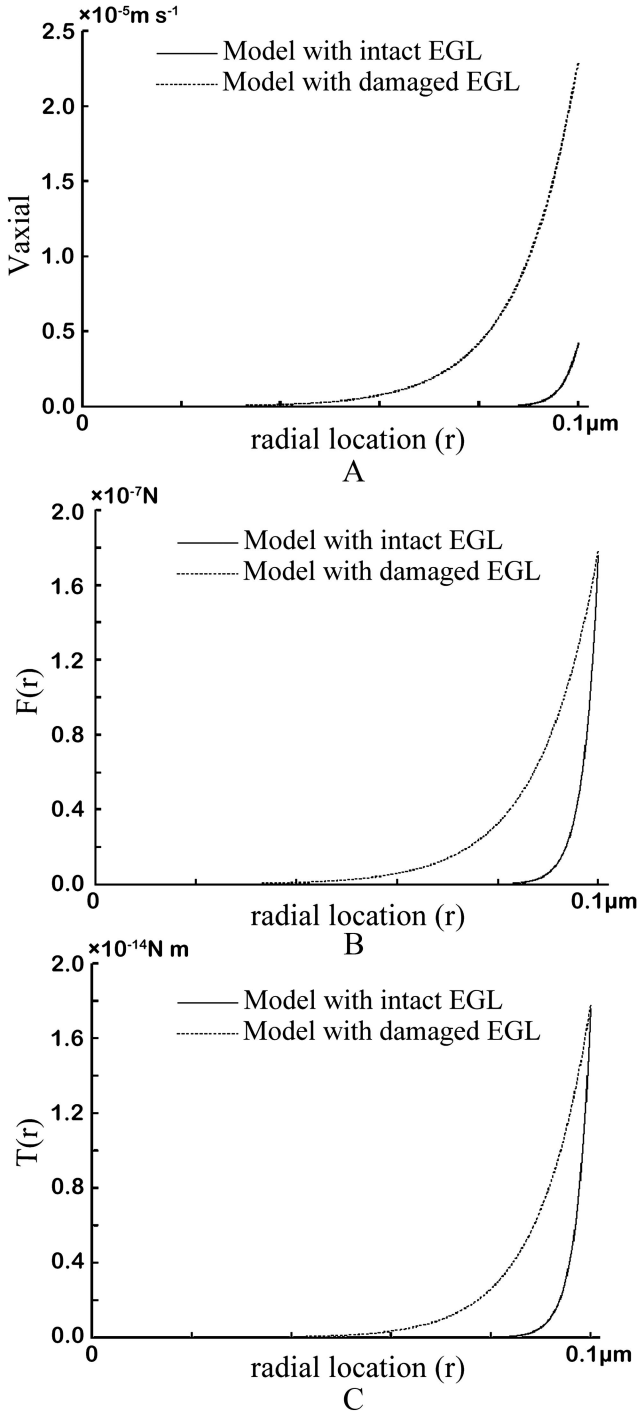

Figure 5. A: The axial velocity profiles across the 0.1 μm endothelial glycocalyx layer (EGL) in models with intact and damaged EGL. **B** and **C**: Comparison of the profiles of the local drag force per unit fiber length ($F(r)$) along the EGL fiber and the bending moment per unit length $T(r)$ acting on the root of the glycocalyx fiber between the damaged EGL model and the intact EGL model.

force acting on the 10 nm top section of a 0.1 μm glycocalyx fiber will drop from 96.4% for the intact model to 57.1%. In addition, the ratio of the corresponding bending moment of the 10 nm section on the root of the fiber to the total torque will also decrease from 96.8% to 61.9%. On the other hand, the

flow-induced shear stress on the membrane of ECs increases drastically from 5.6×10^{-7} to 5.6×10^{-4} Pa.

Effect of EGL Hydraulic Permeability

In the previous set of simulation, we use **Equation 6** to determine the hydraulic permeability of the EGL, in which the flow is assumed to be parallel to the EGL fibers. In reality, however, the flow can go in any direction or even be perpendicular to the fibers. Therefore, in this set of simulation, we use different methods to estimate the hydraulic permeability of the EGL. For the flow perpendicular to a hexagonal array of the circular cylinders, the method proposed by Sangani and Acrivos[26] is used as follows:

$$\frac{K_{\mathrm{egl}}^{\perp}}{r_{\mathrm{f}}^2} = \frac{1\mathrm{n}(c^{-1/2}) - 0.745 + c - c^2/4 + o(c^4)}{4c} \qquad (12)$$

where c is solid fraction of the EGL calculated using **Equation 5**. From **Equation 12**, we have $[K_{\mathrm{egl}}^{\perp}]$ 3.16×10^{-18} m^2.

For the flow in random orientations, the well-known Carman–Kozeny equation is used[27]:

$$\frac{K_{\mathrm{egl}}}{r_{\mathrm{f}}^2} = \frac{(1-c)^3}{4kc^2} \qquad (13)$$

With the Kozeny constant $k = 5.6$, **Equation 13** gives $K_{\mathrm{egl}} = 4.63$ nm^2.

As the EGL is not rigid fibers, the hydraulic permeability of the EGL estimated with the above equations may have some discrepancy with the value in reality. Taking this into consideration, in this set of simulation, we compared three cases with different hydraulic permeabilities, namely 1.0×10^{-18} m^2, 6.0383×10^{-18} m^2, and 1.0×10^{-17} m^2.

As shown in **Figure 6A**, K_{egl} can affect not only the value of $U(R)$ but also the axial velocity profile in the EGL $U(r)$. As K_{egl} increases from 1.0×10^{-18} to 1.0×10^{-17} m^2, $U(R)$increases from 1.73×10^{-6} to 5.50×10^{-6} m $\cdot$ s^{-1} and the ratio of the axial velocity at the location of 10 nm away from the tip to $U(R)$ increases from 3.45% to 7.46%. However, for all hydraulic permeability cases, the filtration rate (the radial velocity) is all approximately 2.89×10^{-8} m $\cdot$ s^{-1}, which is also the value for all the EGL thickness cases.

Figure 6, **B** and **C** demonstrates that the hydraulic permeability of EGL significantly affects the distribution of $F(r)$ and $T(r)$. For both of them, when K_{egl} is lower, they are higher within the 2 nm of the edge of the 0.1 μm ESL. However, deeper within the fiber, when K_{egl} is lower, they are also lower. In addition, it is interesting that the total drag force acting on a glycocalyx fiber and the total torque on the root of a glycocalyx fiber are slightly influenced by the hydraulic permeability of EGL. For the three cases, as K_{egl} increases, the total drag force slightly decreases from 5.40 to 5.32 pN and the total torque also decreases from 5.33×10^{-2} to 5.11×10^{-2} pN $\cdot$ nm.

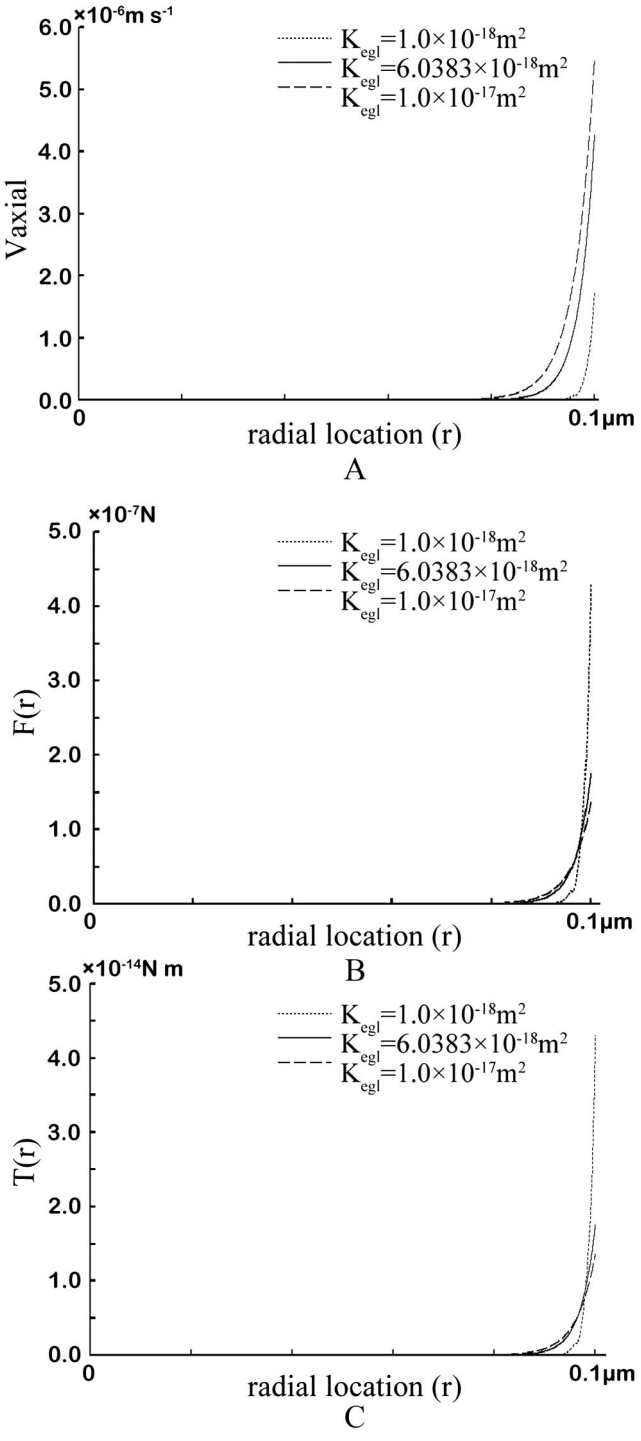

Figure 6. A: The axial velocity profiles across the 0.1 μm endothelial glycocalyx layer (EGL) in models with different K_{egl}. **B** and **C**: The profiles of the local drag force per unit fiber length ($F(r)$) along the EGL fiber and the bending moment per unit length $T(r)$ acting on the root of the glycocalyx fiber in models with different K_{egl}.

Discussion

It has been well recognized that atherosclerotic lesions in the arterial wall develop at certain sites in the human large arteries such as along the inner walls of curved segments and the outer walls of arterial bifurcations.[28] This phenomenon is called the localization of atherosclerosis. Hemodynamic factors such as low flow shear stress and high oscillating shear index have been suggested to play important roles in the localization of atherogenesis.[29–31] Thereby, the responses of ECs to shear stress have been investigated extensively.[1,31–33] However, the underlying mechanotransduction mechanism has not yet been understood clearly. Experimental studies

demonstrated that the EGL lining on the ECs may act as a direct mechanotransducer for flow-induced shear stress.[9–13] This theoretical study lends the support to these observations and indicates that flow-induced shear stress can hardly act on ECs directly but is transmitted to the cells largely by the ESL. Moreover, this study further demonstrates that the damages to the EGL by reducing its thickness or destructing its integrity can hardly affect the total force acting on the membranes of ECs by the glycocalyx fibers. However, such damages can significantly influence the total torque on the roots of the fibers.

The present theoretical modeling shows that the EGL has very little effect on water filtration flow (the radial velocity) across the arterial wall. The simulation shows that for all hydraulic permeability and thicknesses of the EGL studied, the filtration rate remains almost the same as $2.89 \times 10^{-8} m \cdot s^{-1}$, which is higher than the data ($1.78 \times 10^{-8} m \cdot s^{-1}$) measured by Meyer *et al.*[34] but very close to the value ($2.80 \times 10^{-8} m \cdot s^{-1}$) from Tedgui and Lever.[35] This result indicates that the determinate factor in filtration flow is hydraulic pressure and the hydraulic resistance of other layers of the artery, not the EGL itself, indicating that arteries may be very different from capillaries in which the EGL plays an important role in the water balance between capillary and the tissue.[5]

This study revealed that as the axial velocity profile became flat deeper inside the EGL, the shear stress on the cell membrane was negligibly small, which was consistent with the predictions by Weinbaum *et al.*[3] and Secomb *et al.*[6] Our theoretical simulation showed that although partial damage to the EGL caused a dramatic increase in FSS directly acting on the cell's membrane, it was still much smaller than the force transmitted to the cell by the EGL. The results, therefore, indicate that ECs' mechanotransduction of flow-induced shear stress on the endothelial surface is by the glycocalyx fibers of the EGL (no matter intact or partially damaged), not by the direct action of FSS on the cell membranes. It is worth to mention that this result was different from the result of Wang's simulation.[8] Wang showed that when a similar damage to the one in our model occurred to the EGL, the magnitude of the wall shear stress acting on the endothelial surface was comparable with that of the drag force acting on the glycocalyx fibers.

The present simulation also shows that as a large portion of the drag force acted on the tip section of a glycocalyx fiber, the total drag force on a glycocalyx fiber is hardly affected by the thickness of the EGL. However, the changes in the thickness of the EGL may significantly affect the total torque acting on the roots of the glycocalyx fibers, hence affecting the sensing of the cells to flow. In addition, when three quarters of the glycocalyx fibers are removed ($\Delta = 28$ nm), the distribution of the drag force and the bending moment along a glycocalyx fiber is significantly altered due to the elevated porosity and the hydraulic permeability. The corresponding total force on one fiber increases about four times. In this case, the sum of forces acting on the EC by all the fibers does not change (the sum of the forces = the face on one fiber times the number of the fibers), but the sum of the torques on the roots of all the fibers decreases 10%. This, therefore, indicates that when the EGL is damaged either by reducing the thickness of the EGL or by destructing its integrity, the total force on an EC remains almost unchanged, but the total torque on the cell is significantly reduced under the synergic effect of the two types of damages.

Experimental observations seem not to support the idea that the mechanotransduction of shear stress on cells is in the form of forces by the EGL. For instance, Florian *et al.*[9] observed only 45% digestion of HS of EGL by heparinase treatment could completely inhibit the release of NO. Thi *et al.*[36] suggested that 30% reduction of HS was sufficient to inhibit cytoskeletal reorganization induced by shear stress. On the basis of these experimental observations and our theoretical simulation, we believe that the mechanotransduction of shear stress on the ECs might be in torque determined rather than force determined. Given the hypothesis is verified in experiments, such difference might have important clinical implications. For instance, low shear stress has been proposed to be implicated in the formation of localized atherosclerosis in relatively large arteries and the development of restenosis within arteries after a stenting procedure.[29–31,37] Intentional elongation of EGL in the diseased area might amplify the low shear stress and alleviate the atherosclerosis and restenosis. In addition, the components of EGL may act as mechanotransducers for the production of shear stress-induced endothelial NO, which is a well-known potent vasodilator.[38] Therefore, intentional changes in the structure of EGL such as elongating or shortening of EGL might be an effective way to modulate the flow resistance in microvascular vessels.

In this pilot study, we treated the EGL as rigid fibers and ignore the negative charge of the EGL, which may affect the structure of the EGL under shear stress, hence influencing the parameters of the simulation. Nevertheless, *in vivo* observations and theoretical model show that the EGL maintains structural integrity with small deformation when subject to the fluid shear stress of flowing blood.[3,22] In addition, our theoretical modeling demonstrated that although the fluctuation of the EGL hydraulic permeability significantly affected the distribution of the drag force and the bending moment along a glycocalyx fiber, even 10 times of increase in the hydraulic permeability could hardly affect the total force and torque on an EC. The anisotropic permeability of EGL also slightly affected the total force and torque (data not shown in the article). Therefore, although this pilot study has its limitations, it still can shed some lights on the mechanism of EC mechanotransduction for the flow-induced shear stress.

Conclusion

The total force on an EC by the EGL is hardly affected by the damages to the EGL. Nevertheless, the damages can significantly affect the total torque on the EC. We, therefore, propose that the EC mechanotransduction for flow-induced shear stress by the EGL may be trigged by the torques transmitted to the cells from the glycocalyx fibers rather than the forces.

References

1. Hahn C, Schwartz MA: Mechanotransduction in vascular physiology and atherogenesis. *Nat Rev Mol Cell Biol* 10: 53–62, 2009.
2. Tarbell JM, Pahakis MY: Mechanotransduction and the glycocalyx. *J Intern Med* 259: 339–350, 2006.
3. Weinbaum S, Zhang X, Han Y, *et al*: Mechanotransduction and flow across the endothelial glycocalyx. *Proc Natl Acad Sci USA* 100: 7988–7995, 2003.

4. Pries AR, Secomb TW, Gaehtgens P: The endothelial surface layer. *Pflugers Arch* 440: 653–666, 2000.
5. Weinbaum S, Tarbell JM, Damiano ER: The structure and function of the endothelial glycocalyx layer. *Annu Rev Biomed Eng* 9: 121–167, 2007.
6. Secomb TW, Hsu R, Pries AR: Effect of the endothelial surface layer on transmission of fluid shear stress to endothelial cells. *Biorheology* 38: 143–150, 2001.
7. Squire JM, Chew M, Nneji G, *et al*: Quasi-periodic substructure in the microvessel endothelial glycocalyx: A possible explanation for molecular filtering? *J Struct Biol* 136: 239–255, 2001.
8. Wang W: Change in properties of the glycocalyx affects the shear rate and stress distribution on endothelial cells. *J Biomech Eng* 129: 324–329, 2007.
9. Florian JA, Kosky JR, Ainslie K, *et al*: Heparan sulfate proteoglycan is a mechanosensor on endothelial cells. *Circ Res* 93: e136–e142, 2003.
10. Hecker M, Mulsch A, Bassenge E, *et al*: Vasoconstriction and increased flow: Two principal mechanisms of shear stress-dependent endothelial autacoid release. *Am J Physiol* 265: H828–H833, 1993.
11. Kumagai R, Lu X, Kassab GS: Role of glycocalyx in flow-induced production of nitric oxide and reactive oxygen species. *Free Radic Biol Med* 47: 600–607, 2009.
12. Mochizuki S, Vink H, Hiramatsu O, *et al*: Role of hyaluronic acid glycosaminoglycans in shear-induced endothelium-derived nitric oxide release. *Am J Physiol* 285: H722–H726, 2003.
13. Yao Y, Rabodzey A, Dewey CF Jr: Glycocalyx modulates the motility and proliferative response of vascular endothelium to fluid shear stress. *Am J Physiol* 293: H1023–H1030, 2007.
14. Karner G, Perktold K, Zehentner HP: Computational modeling of macromolecule transport in the arterial wall. *Comput Meth Bio-mech Biomed En*g 4: 491–504, 2001.
15. Yang N, Vafai K: Modeling of low-density lipoprotein (LDL) transport in the artery—Effects of hypertension. *Int J Heat Mass Transfer* 49: 850–867, 2006.
16. Zhang X, Curry FR, Weinbaum S: Mechanism of osmotic flow in a periodic fiber array. *Am J Physiol Heart Circ Physiol* 290: H844–H852, 2006.
17. Dabagh M, Jalali P, Tarbell JM: The transport of LDL across the deformable arterial wall: The effect of endothelial cell turnover and intimal deformation under hypertension. *Am J Physiol Heart Circ Physiol* 297: H983–H996, 2009.
18. Lin SJ, Jan KM, Schuessler G, *et al*: Enhanced macromolecular permeability of aortic endothelial cells in association with mitosis. *Atherosclerosis* 73: 223–233, 1988.
19. Song SH, Roach MR: Quantitative changes in the size of fenestration of elastic laminas of sheep thoracic aorta studied with SEM. *Blood Vessels* 20: 145–153, 1983.
20. Lin SJ, Jan KM, Chien S: Role of dying endothelial cells in transendothelial macromolecular transport. *Arteriosclerosis* 10: 703–709, 1990.
21. Tedgui A, Lever MJ: The interaction of convection and diffusion in the transport of 131I-albumin within the media of the rabbit thoracic aorta. *Circ Res* 57: 856–863, 1985.
22. Vink H, Duling BR: Identification of distinct luminal domains for macromolecules, erythrocytes, and leukocytes within mammalian capillaries. *Circ Res* 79: 581–589, 1996.
23. Lewis JC, Taylor RG, Jones ND, *et al*: Endothelial surface characteristics in pigeon coronary artery atherosclerosis. I. Cellular alterations during the initial stages of dietary cholesterol challenge. *Lab Invest* 46: 123–138, 1982.
24. van den Berg BM, Spaan JA, Vink H: Impaired glycocalyx barrier properties contribute to enhanced intimal low-density lipoprotein accumulation at the carotid artery bifurcation in mice. *Pflugers Arch Eur J Physiol* 457: 1199–1206, 2009.
25. van Haaren PM, VanBavel E, Vink H, *et al*: Localization of the permeability barrier to solutes in isolated arteries by confocal microscopy. *Am J Physiol Heart Circ Physiol* 285: H2848–H2856, 2003.
26. Sangani AS, Acrivos A: Slow flow past periodic arrays of cylinders with application to heat transfer. *Int J Multiphase Flow* 8: 193–206, 1982.
27. Happel J, Brenner H (ed): *Low Reynolds Number Hydrodynamics.* Leyden, Noordhoff, 1973.
28. DeBakey ME, Lawrie GM, Glaeser DS, *et al*: Patterns of atherosclerosis and their surgical significance. *Ann Surg* 201: 115–131, 1985.
29. Caro CG, Fitz-Gerald JM, Schroter RC: Atheroma and arterial wall shear. Observation, correlation, and proposal for a shear dependent mass transfer mechanism for atherogenesis. *Proc R Soc Lond B Biol Sci* 117: 109–159, 1971.
30. Ku DN, Giddens DP, Zarins CK, *et al*: Pulsatile flow and atherosclerosis in the human carotid bifurcation. Positive correlation between plaque location and low oscillating shear stress. *Arteriosclerosis* 5: 293–302, 1985.
31. Malek AM, Alper SL, Izumo S: Hemodynamic shear stress and its role in atherosclerosis. *JAMA* 282: 2035–2042, 1999.
32. Davies PF: Flow-mediated endothelial mechanotransduction. *Physiol Rev* 75: 519–560, 1995.
33. Li YS, Haga JH, Chien S: Molecular basis of the effects of shear stress on vascular endothelial cells. *J Biomech* 38: 1949–1971, 2005.
34. Meyer G, Merval R, Tedgui A: Effects of pressure-induced stretch and convection on low-density lipoprotein and albumin uptake in the rabbit aortic wall. *Cir Res* 79: 532–540, 1996.
35. Tedgui A, Lever MJ: Filtration through damaged and undamaged rabbit thoracic aorta. *Am J Physiol Heart Circ Physiol* 247: H784–H791, 1984.
36. Thi M, Tarbell JM, Weinbaum S, *et al*: The role of the glycocalyx in reorganization of the actin cytoskeleton under fluid shear stress: A "bumper-car" model. *Proc Natl Acad Sci USA* 101: 16483–16488, 2004.
37. Thury A, Wentzel JJ, Vinke RV, *et al*: Focal in-stent restenosis near step-up: Roles of low and oscillating shear stress. *Circulation* 105: e185–e187, 2002.
38. Ignarro LJ, Buga GM, Wood KS, *et al*: Endothelium-derived relaxing factor produced and released from artery and vein is nitric oxide. *Proc Natl Acad Sci USA* 84: 9265–9269, 1987.